

Computational simulation of ionization processes in single-bubble and multi-bubble sonoluminescence

Jin-Fu Liang(梁金福), De-Feng Xiong(熊德凤), Yu An(安宇), and Wei-Zhong Chen(陈伟中)

Citation: Chin. Phys. B, 2022, 31 (**11**): 117802. DOI: 10.1088/1674-1056/ac6745

What follows is a list of articles you may be interested in

Computation and analysis of light emission in two-bubble sonoluminescence

Jin-Fu Liang(梁金福), Xue-You Wu(吴学由), Yu An(安宇), Wei-Zhong Chen(陈伟中), Jun Wang(王军)

Chin. Phys. B, 2020, 29 (**9**): 097801. DOI: 10.1088/1674-1056/ab969e

Abnormal ionization in sonoluminescence

Zhang Wen-Juan (张文娟), An Yu (安宇)

Chin. Phys. B, 2015, 24 (**4**): 047802. DOI: 10.1088/1674-1056/24/4/047802

The characteristics of sonoluminescence

An Yu(安宇) and Zhang Wen-Juan(张文娟)

Chin. Phys. B, 2012, 21 (**1**): 017806. DOI: 10.1088/1674-1056/21/1/017806

Computational simulation of ionization processes in single-bubble and multi-bubble sonoluminescence

Jin-Fu Liang(梁金福)[1,†], De-Feng Xiong(熊德凤)[1], Yu An(安宇)[2], and Wei-Zhong Chen(陈伟中)[3]

[1] *School of Physics and Electronic Science, Guizhou Normal University, Guiyang* 550025, *China*
[2] *Department of Physics, Tsinghua University, Beijing* 100084, *China*
[3] *Institution of Acoustics, Nanjing University, Nanjing* 210093, *China*

(Received 5 October 2021; revised manuscript received 9 April 2022; accepted manuscript online 14 April 2022)

The most recent spectroscopic studies of moving-single bubble sonoluminescence (MSBSL) and multi-bubble sonoluminescence (MBSL) have revealed that hydrated electrons (e^-_{aq}) are generated in MSBSL but absent in MBSL. To explore the mechanism of this phenomenon, we numerically simulate the ionization processes in single- and multi-bubble sonoluminescence in aqueous solution of terbium chloride ($TbCl_3$). The results show that the maximum degree of ionization of single-bubble sonoluminescence (SBSL) is approximately 10000 times greater than that of MBSL under certain special physical parameters. The hydrated electrons (e^-_{aq}) formed in SBSL are far more than those in MBSL provided these electrons are ejected from a bubble into a liquid. Therefore, the quenching of e^-_{aq} to SBSL spectrum is stronger than that of the MBSL spectrum. This may be the reason that the trivalent terbium [Tb(III)] ion line intensities from SBSL in the $TbCl_3$ aqueous solutions with the acceptor of e^-_{aq} are stronger than those of $TbCl_3$ aqueous solutions without the acceptor of e^-_{aq}. Whereas the Tb(III) ion line intensities from MBSL are not variational, which is significant for exploring the mechanism behind the cavitation and sonoluminescence.

Keywords: sonoluminescence, Tb(III) ion emission, hydrated electrons, ionization processes

PACS: 78.60.Mq, 47.55.dd, 43.35.+d **DOI:** 10.1088/1674-1056/ac6745

1. Introduction

Single-bubble sonoluminescence (SBSL) is a phenomenon wherein light is emitted during the intense collapse of a single isolated gas bubble driven by a strong ultrasound wave.[1] In contrast, multi-bubble sonoluminescence (MBSL) is the light emission from the intense collapse of clouds of bubbles in liquids by high-intensity ultrasound.[2] At present, it is generally considered that both SBSL and MBSL result from extremely high temperature and pressure conditions that occur during the intense compression heat of gas and vapor in a collapsing bubble.[3–13]

Under such extreme conditions, chemical reactions occur at the inner of the bubble, that is, sonochemistry.[14] Further, the products of the chemical reaction are ejected into the solution from the bubble and may generate subsequent new products, which may affect the characteristics of the spectrum obtained from sonoluminescence (SL),[5,9] sonochemiluminescence (SCL),[15] and sonophotoluminescence (SPL).[16,17]

Recently, Sharipov *et al.* reported the possibility of hydrated electrons (e^-_{aq}) generation upon sonolysis of water in SBSL and the absence of e^-_{aq} in MBSL after they studied the spectra of SBSL and MBSL in solutions of $Ru(bpy)_3^{2+}$[18] and Ce(III)/Ce(IV).[19]

In addition, they confirmed the formation of e^-_{aq} during the moving SBSL (MSBSL) by the activation of Tb(III) ion sonoluminescence owing to e^-_{aq} acceptors in aqueous solution, whereas e^-_{aq} is absent in MBSL in the same solution.[20] This is because the peak temperature achieved during MSBSL is 2000–2500 K higher than that achieved during MBSL, which results in a higher degree of ionization during SBSL than during MBSL. For MSBSL, the electrons ejected from the bubble into the solution form the e^-_{aq} combination with H_2O, while the electronic component of the plasma in the bubble is absent for MBSL. Thus, during MBSL, the generation of e^-_{aq} in the solution does not allow the sonolysis products to eject from the bubble into the solution more effectively than during MSBSL. However, the process of generating electrons in an MSBSL and the reason for the absence of electron components in the plasma in the bubble remain unknown. In this study, we simulate the ionization processes in SBSL and MBSL, which further illustrates the difference in e^-_{aq} generation between the SBSL and MBSL.

2. Theoretical model

2.1. SBSL theoretical model

The SBSL model employed herein is similar to that reported in previous studies.[10,21–23] The dynamic computation of the sonoluminescent bubble motion involves solving the equation of radial motion of the bubble wall, which is referred to as Keller–Miksis (KM) equation, in conjunction with the fluid mechanics equation, the formula of water evaporation and vapor condensation at the bubble wall, and the energy equation in liquid for exterior temperature evaluation.

†Corresponding author. E-mail: jfliang@gznu.edu.cn

© 2022 Chinese Physical Society and IOP Publishing Ltd

The KM equation describes the radiation motion of the bubble wall,[24,25] expressed as

$$(1-M)R\ddot{R}+\frac{3}{2}\left(1-\frac{M}{3}\right)\dot{R}^2 = (1+M)\frac{1}{\rho_{\rm l}}(p_{\rm l}-p_\infty-p_{\rm s}(t+t_R))+\frac{t_R}{\rho_{\rm l}}\dot{p}_{\rm l}, \quad (1)$$

where $M\equiv\dot{R}/c_{\rm l}$ is the bubble wall Mach number, representing the effects caused by the compressibility of the liquid, $R\equiv R(t)$ is the radius of the bubble, $\dot{R}$ is the speed of the bubble wall, and $c_{\rm l}$ is the speed of sound in the liquid. The $\cdot$ and $\cdot\cdot$ operators denote the first and second order derivatives with respect to time t, respectively. Further, $\rho_{\rm l}$ is the liquid density on the liquid side of the bubble wall. $p_{\rm l}=p_{\rm g}-4\eta\frac{\dot{R}}{R}-\frac{2\sigma}{R}$ is the pressure on the liquid side of the bubble wall, where η is the dynamic viscosity, and σ is the surface tension coefficient of the liquid. p_∞ is the ambient pressure, $p_{\rm g}=\frac{\mu\mathscr{R}T}{V-b}+p_{\rm v}$, where μ, $\mathscr{R}$, and T represent the gas mole number, gas constant, and temperature of the surrounding liquid, respectively. $V=4\pi R^3/3$ is the bubble volume, where b and $p_{\rm v}$ denote the van der Waals hard core volume and vapor pressure of the liquid, respectively. $p_{\rm s}(t)=-p_{\rm a}\sin(2\pi ft)$ is the driving acoustic pressure, and $p_{\rm a}$ is the amplitude of the sound pressure. Further, f is the frequency of the acoustic wave, $t_R=R/c_{\rm l}$.

To simulate the ionization processes occurring inside a bubble, we consider the chemical dissociation reactions as follows:[10]

$$\rm H_2O\leftrightarrow OH+H, \quad (2)$$
$$\rm OH\leftrightarrow O+H, \quad (3)$$
$$\rm H+H\leftrightarrow H_2, \quad (4)$$
$$\rm O+O\leftrightarrow O_2, \quad (5)$$

and the ionization process

$$M\leftrightarrow M^+ +\rm e, \quad (6)$$

where M denotes argon (Ar) and the atoms and molecules appearing in Eqs. (2)–(5). Further, the processes of the attachment of electrons to hydrogen and oxygen atoms or related molecules is expressed as

$$M+\rm e\leftrightarrow M^-, \quad (7)$$

where M^- represents the negative ions $\rm O^-$, $\rm H^-$, $\rm O_2^-$, and $\rm OH^-$. The law of mass action can be used to evaluate the number density of the products of the chemical dissociation and ionization electrons, as well as the positive and negative ions. The processes of the radiative attachment of electrons to atoms or molecules or ions are expressed as

$$\rm O+e\leftrightarrow O^-+h\nu, \quad (8)$$
$$\rm H+e\leftrightarrow H^-+h\nu, \quad (9)$$
$$\rm O_2+e\leftrightarrow O_2^-+h\nu, \quad (10)$$
$$\rm OH+e\leftrightarrow OH^-+h\nu, \quad (11)$$

where $h=6.626\times10^{-34}$ J·s is the Planck constant, $\nu=c/\lambda$, and $c=3.0\times10^8$ m/s is the speed of light, and λ is wavelength of light. The total radiation power is the integral over the relevant wavelength λ [10,23] as

$$P(t)=\int_{200\ \rm nm}^{900\ \rm nm}P(\lambda,t)\,{\rm d}\lambda, \quad (12)$$

where

$$P(\lambda,t) = 8\pi^2\int_0^R\int_{-1}^1 k_\lambda(r)P_\lambda^{\rm PI}(r) \times\exp\left(-\int_{r_x}^{\sqrt{R^2-r^2(1-x^2)}}k_\lambda\,{\rm d}s\right)r^2\,{\rm d}r\,{\rm d}x, \quad (13)$$

which describes the total power emitted from the bubble for each acoustic cycle at a wavelength λ. Further, in Eq. (13), r is the radial distance from the center of the bubble, k_λ is the absorption coefficient, and $P_\lambda^{\rm PI}$ is the Plank radiation intensity[26]

$$P_\lambda^{\rm PI}(r)=\frac{2\pi hc^2}{\lambda^5}\frac{1}{\exp(hc/\lambda k_{\rm B}T)-1}, \quad (14)$$

where $k_{\rm B}$ denotes the Boltzmann constant.

For the line emission from Tb(III), the absorption coefficient is expressed as

$$k_\lambda=\frac{\lambda^5}{2hc^2}(\mathrm{e}^{hc/\lambda kT}-1)P_\lambda, \quad (15)$$

where P_λ represents the radiation power per unit volume per unit wavelength interval of the line spectrum. Herein, we mainly consider the $^5{\rm D}_4\rightarrow{}^7{\rm F}_J$ ($J=6,5,4,\ldots,0$) transitions of Tb(III).

In addition, Eq. (16) expresses the cumulative radiation energy emitted from a sonoluminescent bubble over time 0 to t within each acoustic period as

$$E_\lambda(t)=\int_0^t P(\lambda,t')\,{\rm d}t',\quad 0\le t\le\frac{2\pi}{\omega}. \quad (16)$$

2.2. MBSL theoretical model

A bubble in the MBSL construct may pulse at one location over an acoustic period, even though it is subjected to the pressure from other bubbles. The wall of a bubble among dense cavitation bubbles is determined by using the modified KM equation[28]

$$(1-M_i)R_i\ddot{R}_i+\frac{3}{2}\left(1-\frac{M_i}{3}\right)\dot{R}_i^{\,2} = (1+M_i)\frac{1}{\rho_{\rm l}}(p_{{\rm l}i}-p)+\frac{t_R}{\rho_{\rm l}}\dot{p}_{{\rm l}i}, \quad (17)$$

where $M_i\equiv\frac{\dot{R}_i}{c_{\rm l}}$, $p_{{\rm l}i}=p_{{\rm g}i}-4\eta\frac{\dot{R}_i}{R_i}-\frac{2\sigma}{R_i}$, $p_{{\rm g}i}=\frac{\mu\mathscr{R}T}{V_i-b}+p_{\rm v}$, $V_i=\frac{4\pi R_i^3}{3}$, $t_{R_i}=\frac{R_i}{c_{\rm l}}$ and the pressure p of driving the bubble at a location in the liquid is employed in the equation for cavitation cloud, expressed as follows:[27,28]

$$\nabla^2p-\frac{1}{c_{\rm l}^2}\frac{\partial^2p}{\partial t^2}=-4\pi\rho_{\rm l}\sum_i N_i(2R_i\dot{R}_i^{\,2}+R_i^2\ddot{R}_i), \quad (18)$$

where N_i is the number density of cavitation bubbles with the initial radius R_{i0}. Based on the Eqs. (17) and (18), we can obtain the pressure distribution by numerical calculation. The pressure driving the bubble at a location in liquid is derived approximatively. In present paper, we consider that the MBSL and SBSL constructs have the same chemical dissociation reactions and ionization processes in a bubble.

3. Results and discussion

In the present study, certain parameters in the experiment conducted by Sharipov[20] were referenced in the numerical calculation. Table 1 lists the parameters used.

Table 1. Parameters used in the numerical simulation.

Variable (unit)	SBSL	MBSL
T_0 (K)	273	278
R_{i0} (μm)	4.8	4.8
f (kHz)	26	20
p_a (atm)	1.34	2.5
N_i (m^{-3})		3×10^9
c_l (ms^{-1})	1481	1481
ρ_l (kgm^{-3})	1000	1000
η (Pa·s)	0.0017	0.001
σ ($N{\cdot}m^{-1}$)	0.075	0.0725
p_∞ (atm)	1.0	1.0
γ	1.4	1.4

3.1. Plasma in a single sonoluminescent bubble

To understand the process of plasma formation in the SBSL bubble, we simulated the light emission pulse inside an Ar bubble in an aqueous solution of $TbCl_3$ at 0 °C, driven by an acoustic pressure of 1.34 atm.

Figure 1(a) illustrates the total radiation power per flash of the simulated bubble. Five moments (points marked A–E) were selected on the cure to evaluate the temperature [Fig. 1(b)], corresponding pressure [Fig. 1(c)], radiation energy spectra [Fig. 1(d)], and the number density of various particles inside a bubble [Fig. 2]. Figure 1 depicts that as the radiation power increases from A to D [Fig. 1(a)], the temperature [Fig. 1(b)] and pressure [Fig. 1(c)] inside the bubble, as well as the intensity of the continuum background, increase; the OH, Ar^+, and Tb(III) spectral peaks gradually disappear [Fig. 1(d)].

Because the radiation energy spectrum accumulates over time, the total intensity increases at each moment. In addition, at every moment, the maximum temperature generates at the center of bubble, and intense decreases at the wall of bubble [Fig. 1(b)]. While the pressure inside the bubble is almost

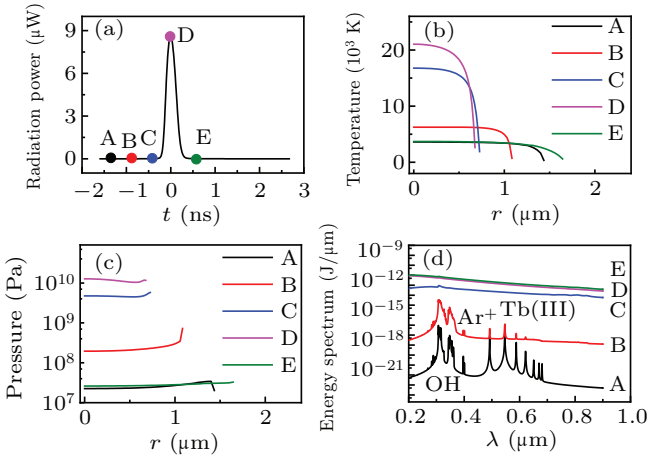


Fig. 1. Simulation results for an Ar bubble in a $TbCl_3$ aqueous at 0 °C, driven by an acoustic pressure amplitude of 1.34 atm. (a) Radiation power of the bubble versus time. (b) Temperature. (c) Pressure. (d) Energy spectrum.

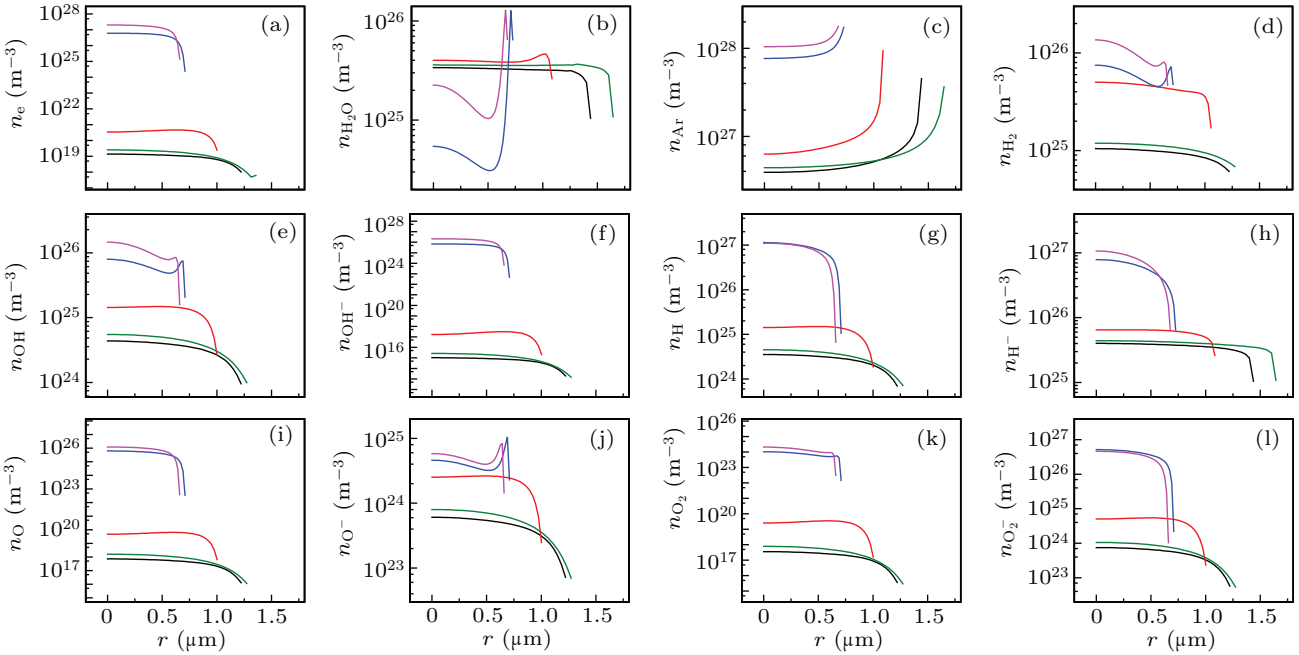


Fig. 2. Spatial profiles of the calculated number densities of various particles filled circles in Fig. 1(a). (a) e^-, (b) H_2O, (c) Ar, (d) H_2, (e) OH, (f) OH^-, (g) H, (h) H^-, (i) O, (j) O^-, (k) O_2, and (l) O_2^-. The black, red, blue, megenta and olive lines corresponds to A, B, C, D, and E in Fig 1(a), respectively.

uniform [Fig. 1(c)]. The reason may be the effects caused by the thermal conductivity of gas and compressibility of the liquid.

Figures 2 illustrates the spatial variations of the number densities of the various particles inside a bubble. Inside the bubble, except for those of the H_2O molecules [Fig. 2(b)] and Ar atoms [Fig. 2(c)], the maximum number densities of other particles occur at the center of the bubble throughout the cycle, and subsequently decreases precipitously in the vicinity of the bubble wall.

To illustrate the generating in SBSL in $TbCl_3$ aqueous solution, the ionized electron density should be considered by assuming that the reaction process occurs during water sonolysis,[20]

$$H_2O \quad))) \rightarrow H_2O^+ + e^- \xrightarrow{H_2O} OH^* + H^+ + e^-_{aq}. \qquad (19)$$

The ionized electron density was positively correlated with temperature. When the bubble reached its maximum temperature of approximately 21000 K [corresponding to the D megenta line in Fig. 1(b)], the ionized electron density reached approximately 2×10^{27} m^{-3} [Fig. 2(a)].

3.2. Plasma in a bubble among sonoluminescencing multi-bubble

Firstly, we calculated the evolution of the pressure field and bubble radii with time [Fig. 3] in the MBSL condition using Eqs. (17) and (18). For simplicity, we consider only one bubble, with an ambient radius of R_{i0}. The number density (N_i) of bubbles is homogeneous in the $TbCl_3$ aqueous solution. The calculation method was similar to that described in previous studies.[29,30]

Figure 3 presents the evolution of pressure and bubble radius with time at three locations N_1 $(r,z) = (0, 0.2$ cm), N_2 (0.5 cm, 0.2 cm), and N_3 (0, 0.7 cm) shown in Fig. 4. The pressure was periodically pulsed with an ultrasound frequency of 20 kHz [Figs. 3(a), 3(b), 3(e), 3(f), 3(i), and 3(j)]. Further, the radius of the bubble in the MBSL exhibits period motion wherein the bubble expands, intensely collapses, and bounces with an ultrasound frequency of 20 kHz [Figs. 3(c), 3(d), 3(g), 3(h), 3(k) and (l)]. Additionally, the pressure peak of each pulse corresponds to the minimum radius of the collapsing bubble, which is exhibited in the fluctuation of the pulsation of the bubble. This indicates that the same type of bubbles are in synchronous resonance near the horn tip (approximately 1 cm).

To determine the region of MBSL in the sound field, we estimated the light intensity of the sonoluminescent bubble by introducing a specific value, R_{max}/R_{i0}. Here, R_{max} represents the maximum radius of a bubble driven by the sound field. Generally, SBSL can be observed by the naked eye when $R_{max}/R_{i0} \geq 5$. However, in this study, we introduced this ratio to estimate the area of the MBSL.[29,30] Figure 4 illustrates that when $0 \leq z \leq 0.6$ cm, and $0 \leq r \leq 0.5$ cm, light emission can be observed from the bubbles in the acoustic field region.

We used an existing method[10,29,30] to illustrate the ionization processes in one sonoluminescent bubble among the cavitation bubbles. The light pulse, number densities of various particles, and degree of ionization (α) inside a bubble at different locations in the sound field were also calculated.

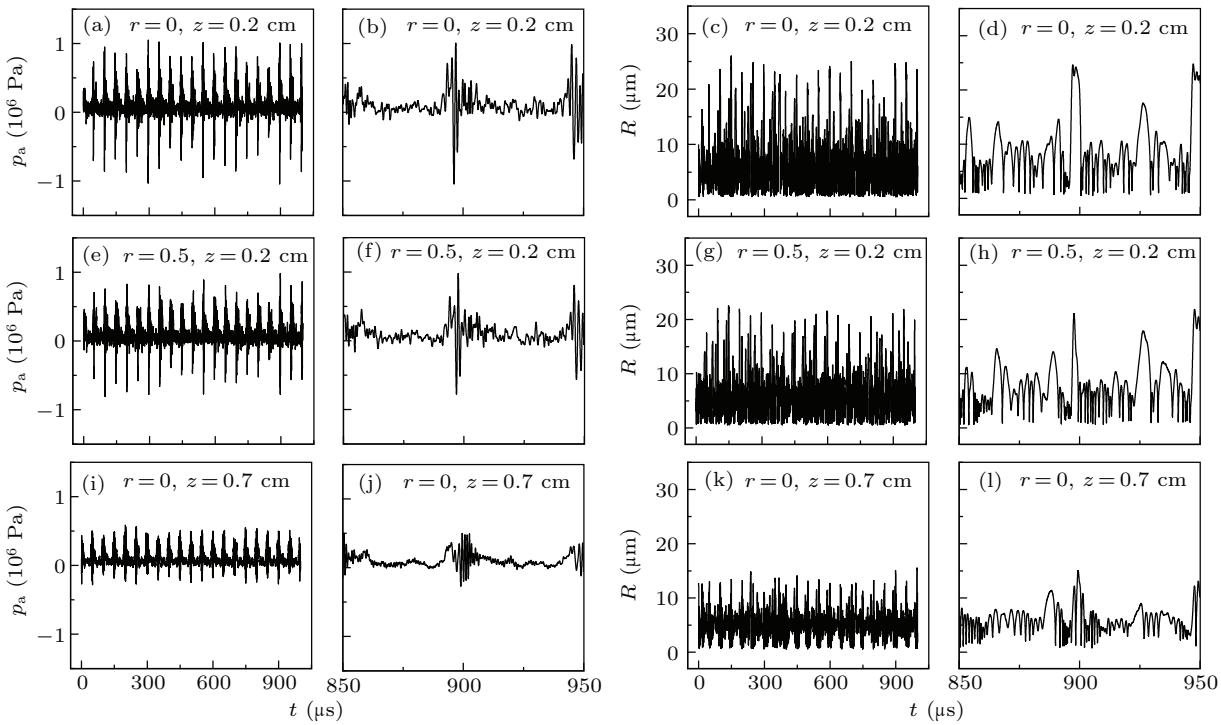


Fig. 3. Evolution of acoustic pressure and bubble radius with t. Results at location (a)–(d) N_1 ($r = 0$, $z = 0.2$ cm), (e)–(h) N_2 ($r = 0.5$ cm, $z = 0.2$ cm), and (i)–(l) N_3 ($r = 0$, $z = 0.7$ cm).

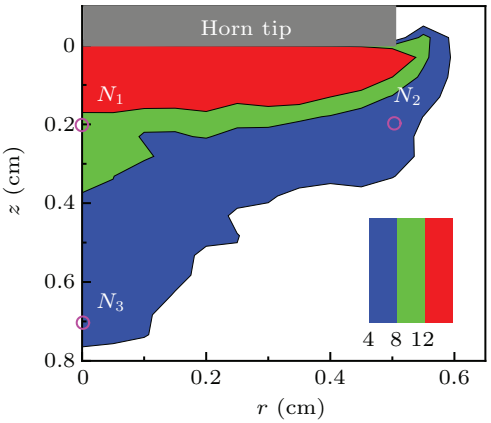


Fig. 4. Contour of close to the horn. The magenta cycles correspond to locations N_1 ($r = 0$, $z = 0.2$ cm), N_2 ($r = 0.5$ cm, $z = 0.2$ cm), and N_3 ($r = 0$, $z = 0.7$ cm).

Figure 5(a) illustrates the total radiation power per flash of the bubble at location N_1 $(r,z) = (0, 0.2$ cm) in the sound field, and five moments (points marked A–E) were selected to evaluate the temperature [Fig. 5(b)], pressure [Fig. 5(c)], radiation energy spectrum [Fig. 5(d)], and the corresponding number densities of various particles [Fig. 6]. In Fig. 6, except for those of the H_2O molecules [Fig. 6(b)] and Ar atoms [Fig. 6(c)], the maximum number densities of other particles occur at the center of the bubble throughout the cycle, and subsequently decreases precipitously in the vicinity of the bubble wall. SBSL also exhibited a similar phenomenon [Fig. 2]. When the bubble reached its maximum temperature of approximately 21000 K [Fig. 5(b)], the ionized electron density reached approximately 2×10^{27} m^{-3} [D megenta line in Fig. 6(a)]. If these electrons are ejected into the solution to combine with H_2O, e^-_{aq} is formed in the solution. However, in the experiment, the e^-_{aq} was absent when analyzing the spectrum lines of Tb(III) ions. This is probably because most of the bubbles are broken when they cannot reach their minimum radii, and the temperature inside cannot attain a sufficient value to ionize more electrons. The experimental data presented in a previous study[31,32] concluded that the temperature inside the bubble in MBSL in water reaches approximately 5000 K, which approaches to the temperature at moment point C, as depicted in Fig. 5(a). At point B, the ionized electrons are approximately 6×10^{24} m^{-3} [red line in Fig. 6(a)].

To further explore the plasma inside a bubble at other locations in the sound field, we simulated the light emission

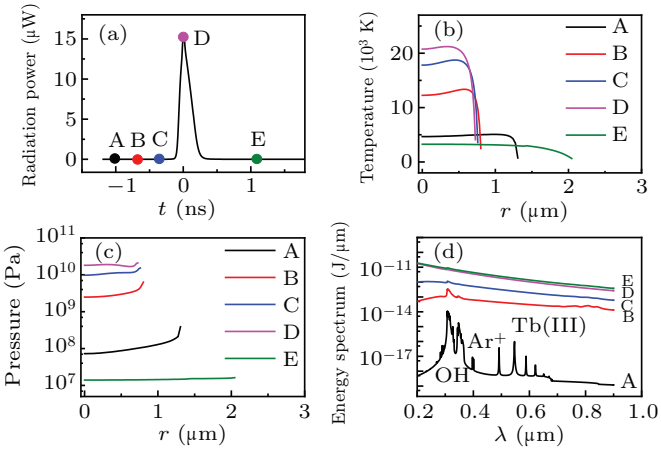


Fig. 5. Simulation results of an argon bubble at the location N_1 ($r = 0$, $z = 0.2$ cm) during the 18th acoustic cycle (850–900 s) demonstrated in Fig. 3(b). The number density of Tb(III) ions is $n\times10^{-5}$. n is the total number density of particles inside a bubble. (a) Radiation power of the bubble versus time. (b) Temperature. (c) Pressure. (d) Energy spectrum.

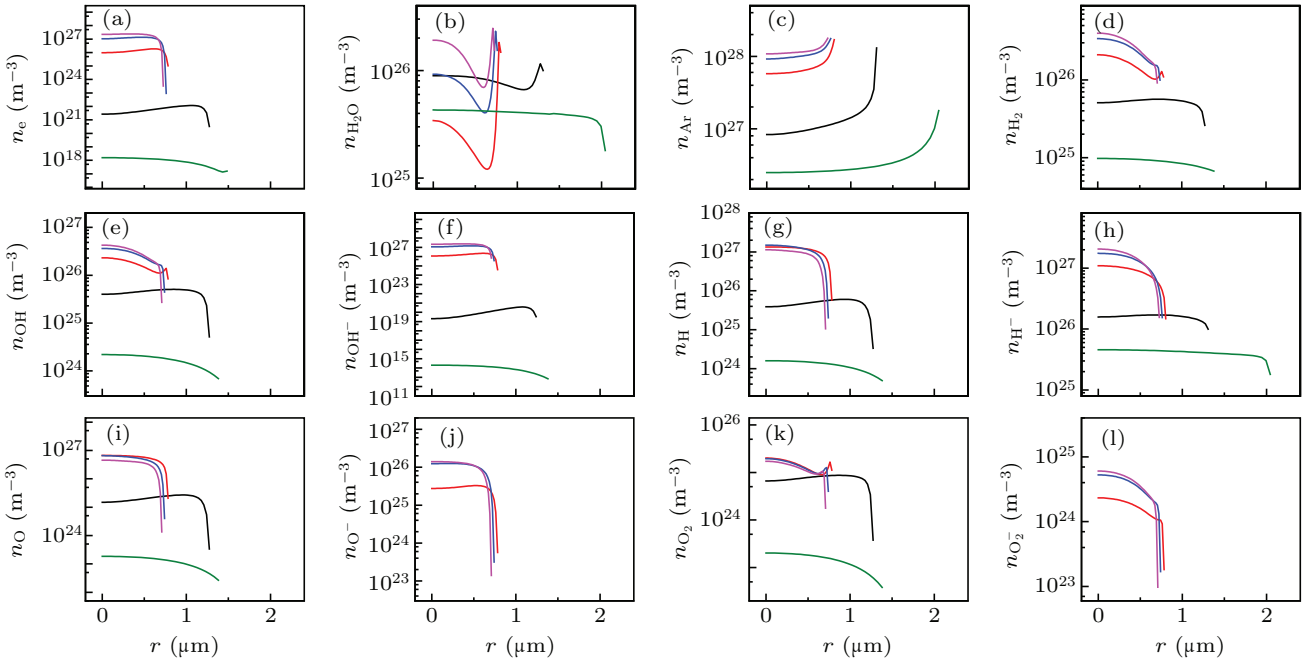


Fig. 6. Spatial profiles of the calculated densities of various particles at the given points of A, B, C, D, E denoted by filled circles in Fig. 5(a). (a) e^-, (b) H_2O, (c) Ar, (d) H_2, (e) OH, (f) OH^-, (g) H, (h) H^-, (i) O, (j) O^-, (k) O_2, and (l) O_2^-. The black, red, blue, megenta and olive lines corresponds to A, B, C, D, and E in Fig 5(a), respectively.

pulse, temperature, pressure, radiation energy spectra, and the number density of various particles inside an Ar bubble at two locations N_2 $(r,z) = (0.5\ \text{cm}, 0.2\ \text{cm})$ and N_3 (0, 0.7 cm). Figures 7 and 8 illustrate the case for the bubble at N_2 $(r,z) = (0.5\ \text{cm}, 0.2\ \text{cm})$.

Figure 7(a) demonstrates the total radiation power per flash of the bubble, and five moments (points marked A–E) were selected to evaluate the temperature [Fig. 7(b)]), pressure [Fig. 7(c)], radiation energy spectrum [Fig. 7(d)], and the corresponding number densities of various particles [Fig. 8]. Figure 7(b) depicts that the maximum temperature inside the bubble is approximately 5800 K, approaching the experimental value of 5000 K, as reported in previous studies.[31,32] The corresponding maximum ionization electrons were approximately 4×10^{22} m^{-3} [megenta line in Fig. 8(a)], which is approximately 10^4 times less than that in SBSL [bule line in Fig. 2(a)].

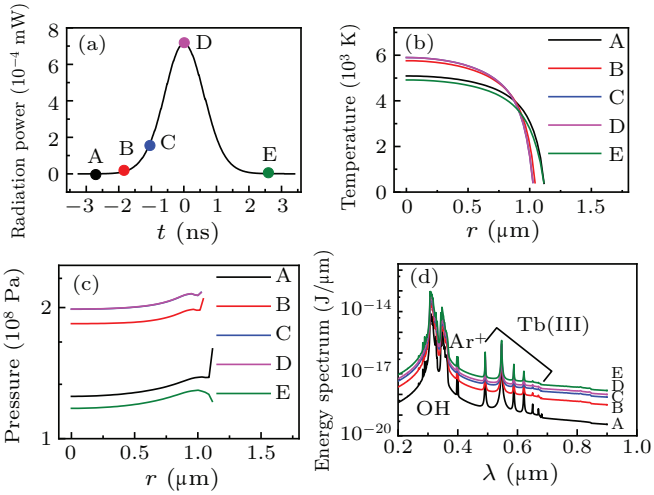


Fig. 7. Simulation results of an Ar bubble at the location N_2 ($r = 0.5$ cm, $z = 0.2$ cm) during the 18$^{\text{th}}$ acoustic cycle (850–900 s) depicted in Fig. 3(f). The number density of Tb(III) ions is $n \times 10^{-5}$. (a) Radiation power of the bubble versus time. (b) Temperature. (c) Pressure. (d) Energy spectrum.

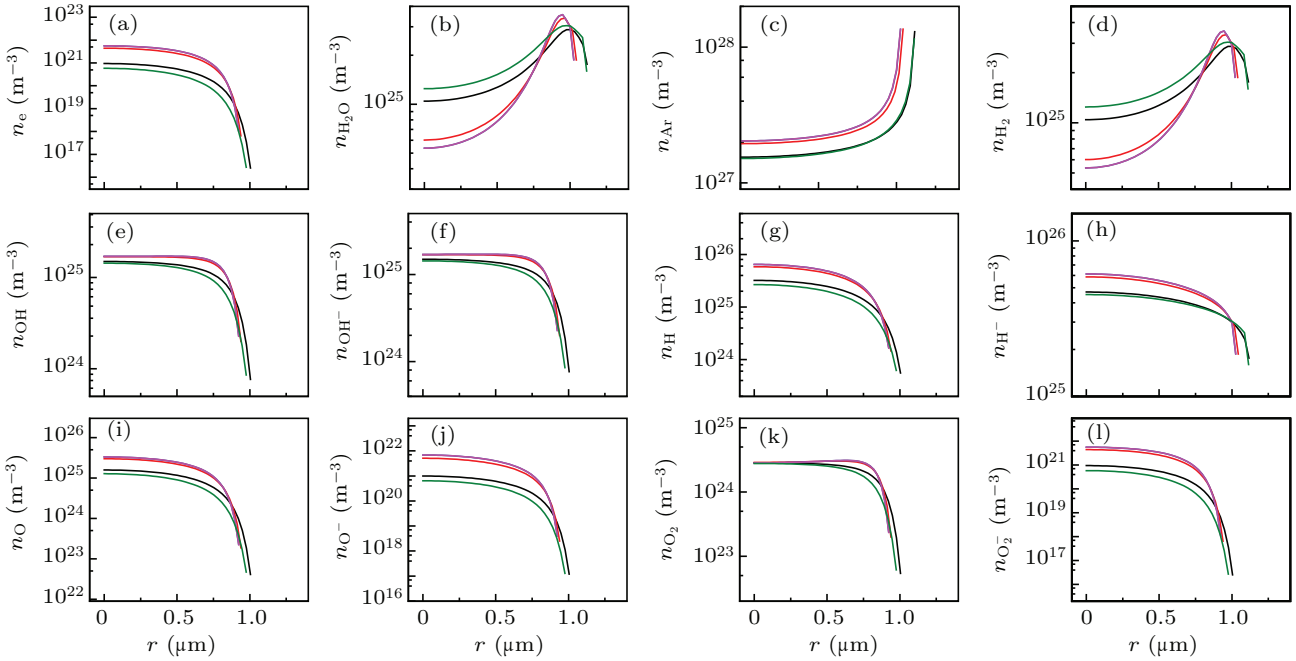


Fig. 8. Spatial profiles of the calculated densities of various particles at the given points of A, B, C, D, E denoted by filled circles in Fig. 7(a). (a) e^-, (b) H_2O, (c) Ar, (d) H_2, (e) OH, (f) OH^-, (g) H, (h) H^-, (i) O, (j) O^-, (k) O_2, and (l) O_2^-. The black, red, blue, megenta and olive lines corresponds to A, B, C, D, and E in Fig 7(a), respectively.

Figures 9 and 10 illustrate the case where the bubble is at the location N_3 $(r,z) = (0, 0.7\ \text{cm})$. Figure 9(a) shows the total radiated power per flash of the bubble, and five moments were selected (points marked A–E) on the curve to evaluate the temperature [Fig. 9(b)], pressure [Fig. 9(c)], radiation energy spectrum [Fig. 9(d)], and the corresponding number of densities of various particles, which is similar to the cases of the bubbles located at the points N_1 (0, 0.2 cm) and N_2 (0.5, 0.2 cm). As depicted in Fig. 9(b), the maximum temperature inside the bubble was approximately 3800 K, less than the experimental value of 5000 K,[31,32] and the corresponding maximum ionized electrons were approximately 2×10^{20} m^{-3} [megenta line in Fig. 10(a)].

To further understand the ionization processes inside a bubble, we calculated the degree of ionization (α) in SBSL and MBSL. Figures 11(a) and 11(b) show α at different moments for SBSL and MBSL at location N_1 (0, 0.2 cm), respectively. The maximum α occurs at the center of the bubble throughout the cycle, and subsequently decreases in the vicinity of the bubble wall.

Figure 12 illustrates the spatial profiles of α at the maximum temperature corresponding to the minimum radius of the bubble for SBSL and at locations N_1 (0,0.2 cm), N_2 (0.5, 0.2 cm), and N_3 (0, 0.7 cm) in the sound field generating MBSL. As depicted in Fig. 12, the maximum α inside a bubble at location N_1 (0. 0.2 cm) was slightly more than that in

SBSL. However, the temperature after fitting the experimental MBSL spectrum[30,31] was far less than the calculated temperature [Fig. 5(b)]. Further, the temperature obtained by fitting the experimental spectrum is close to the calculated temperature inside a bubble at N_2 (0.5, 0.2 cm). Therefore, we consider α inside a bubble at locations N_2 (0.5, 0.2 cm) as that in MBSL.

Figure 12 illustrates that α in SBSL is approximately 10000 times greater than that in MBSL (only for the bubble at location N_2). Assuming that α is generated similarly for both SBSL and MBSL by combining the ionized electrons with H_2O, the number density of e_{aq}^- formed in the solution for SBSL is considerably higher than that for MBSL. Therefore, the quenching of e_{aq}^- to Tb(III) line emission from SBSL is stronger than that from MBSL,[20] which possibly explains the absence of e_{aq}^- in MBSL.

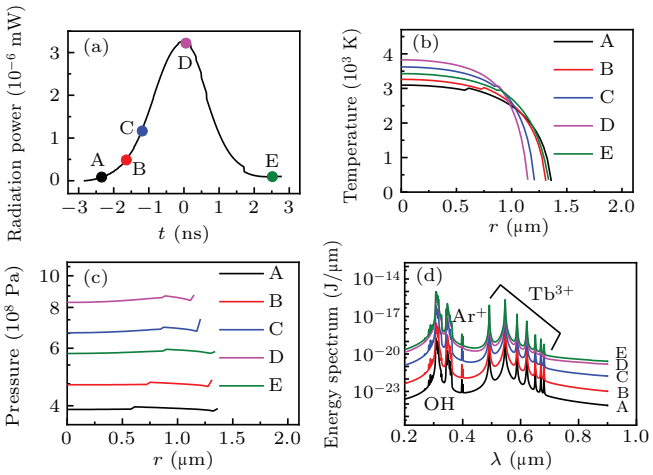


Fig. 9. Simulation results of an Ar bubble at the location N_3 ($r = 0$, $z = 0.7$ cm) during the 18th acoustic cycle (850–900 s) illustrated in Fig. 3(j). The number density of Tb(III) ions is $n \times 10^{-5}$. (a) radiation power of the bubble versus time. (b) Temperature. (c) Pressure. (d) Energy spectrum.

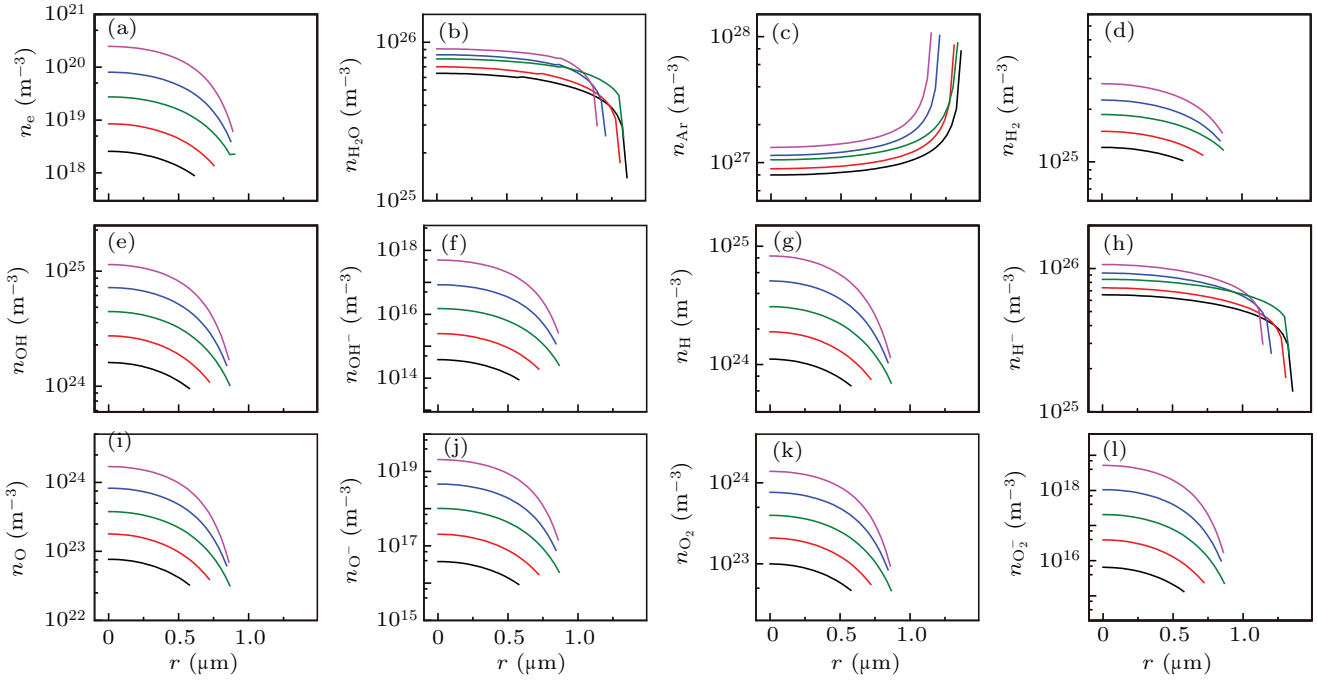


Fig. 10. Spatial profiles of the calculated densities of various particles at the given points of A, B, C, D, E denoted by filled circles in Fig. 9(a). (a) e^-, (b) H_2O, (c) Ar, (d) H_2, (e) OH, (f) OH^-, (g) H, (h) H^-, (i) O, (j) O^-, (k) O_2, and (l) O_2^-. The black, red, blue, megenta and olive lines corresponds to A, B, C, D, and E in Fig 9(a), respectively.

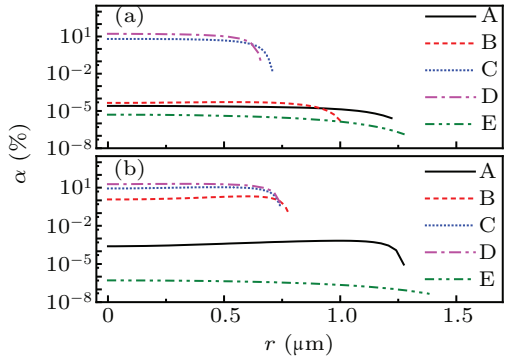


Fig. 11. Variation of the calculated degree of ionization α with r inside a bubble. (a) Corresponds to the moments A, B, C, D, E marked in Fig. 1(a). (b) Corresponds to the moments A, B, C, D, E marked in Fig. 5(a).

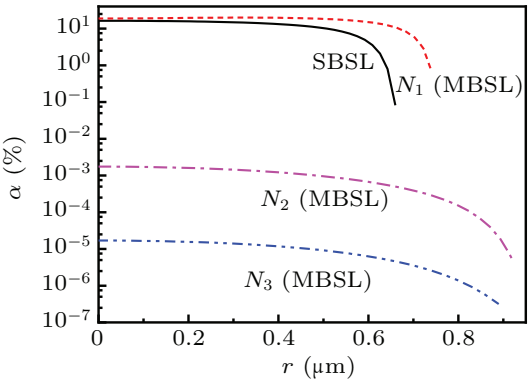


Fig. 12. Comparison of the calculated degrees of ionization.

4. Conclusion

We obtained the total radiated power and energy spectra from SBSL and MBSL, respectively. The corresponding spatial profiles of temperature, pressure, number densities of various particles, and degree of ionization inside an Ar bubble were also obtained. Under certain special conditions, the degree of ionization in SBSL (generated by $p_a = 1.34$ atm and $f = 26$ kHz) was approximately 10000 times greater than that in MBSL (generated by $p_a = 2.5$ atm and $f = 20$ kHz). However, certain parameters in our calculations, such as the number density of bubbles (N) and type of bubble, were assumed instead of being calculated through experiments. In addition, we did not consider the contribution of SPL to Tb(III) ion line emission, which results in a slight difference in the profile between the experimental[17,33,34] and calculated spectra in SBSL.

Acknowledgement

Project supported by the National Natural Science Foundation of China (Grant Nos. 11864007 and 11564006).

References

[1] Gaitan D F, Crum L A, Church C C and Roy R A 1992 *J. Acoust. Soc. Am.* **91** 66
[2] Frenzel H and Schultes H 1934 *Z. Phys. Chem. B* **27** 421
[3] Flint E B and Suslick K S 1991 *Science* **253** 1397
[4] Hilgenfeldt S, Grossmann S and Lohse D 1999 *Nature* **398** 402
[5] Yasui K 2001 *Phys. Rev. E* **64** 0160
[6] Lohse D, Brenner M P, Dupont T F, Hilgenfeldt S and Johnston B 1997 *Phys. Rev. Lett.* **78** 1359
[7] Young J B, Nelson J A and Kang W 2001 *Phys. Rev. Lett.* **86** 2673
[8] Brenner M P, Hilgenfeldt S and Lohse D 2002 *Rev. Mod. Phys.* **74** 425
[9] Flannigan D J and Suslick K S 2005 *Nature* **434** 52
[10] An Y 2006 *Phys. Rev. E* **74** 026304
[11] Suslick K S and Flannigan D J 2008 *Annu. Rev. Phys. Chem.* **59** 659
[12] Xu H, Glumac N and Suslick K 2010 *Angew. Chem. Int. Edit.* **49** 1079
[13] Iii M N, Didenko Y T and Suslick K S 1999 *Nature* **401** 772
[14] Neppiras E A 1980 *Phys. Rep.* **61** 159
[15] Suslick K S and Flint E B 1987 *Nature* **330** 553
[16] Ashokkumar M and Grieser F 1998 *Chem. Commum.* 561
[17] Pflieger R, Schneider J, Siboulet B, Moehwald H and Nikitenko S 2013 *J. Phys. Chem. B* **117** 2979
[18] Sharipov G L, Yakshembetova L R, Abdrakhmanov A M and Gareev B M 2019 *Ultrason. Sonochem.* **58** 104674
[19] Sharipov G L, Gareev B M, Vasilyuk K S, Galimov D I and Abdrakhmanov A M 2020 *Ultrason. Sonochem.* **70** 1053
[20] Sharipov G L, Gareev B M and Abdrakhmanov A M 2020 *J. Photoch. Photobio. A* **402** 112800
[21] An Y and Li C 2008 *Phys. Rev. E* **78** 0463
[22] An Y and Li C 2009 *Phys. Rev. E* **80** 046320
[23] Liang J and An Y 2017 *Phys. Rev. E* **96** 0618
[24] Keller J B and Miksis M 1980 *J. Acoust. Soc. Am.* **68** 628
[25] Zhang W J, Chen W and An Y 2015 *Chin. Phys. B* **24** 047802
[26] Yuan L 2005 *Phys. Rev. E* **72** 046309
[27] Hamilton M F, Ilinskii Y A and Zabolotskaya E A 1998 *Dispersion in nonlinear acoustics* (San Diego: Academic Press)
[28] An Y 2012 *Phys. Rev. E* **85** 016305
[29] An Y 2013 *Appl. Acoust.* **85** 016305 (in Chinese)
[30] Liang J, An Y and Chen W 2019 *Ultrason. Sonochem.* **58** 104688
[31] Didenko Y T, McNamara W B and Suslick K S 1999 *J. Am. Chem. Soc* **121** 5817
[32] Didenko Y T 1999 *J. Phys. Chem. A* **103** 10783
[33] Liang J, Chen W, Zhou C, Cui W and Chen Z 2015 *Phys. Lett. A* **379** 497
[34] Liang J, Chen W, Wang X, Yang J and Chen Z 2016 *Phys. Lett. A* **380** 4105